This is the accepted manuscript made available via CHORUS. The article has been published as:

Subcycle Dynamics of Coulomb Asymmetry in Strong Elliptical Laser Fields

Min Li, Yunquan Liu, Hong Liu, Qicheng Ning, Libin Fu, Jie Liu, Yongkai Deng, Chengyin Wu, Liang-You Peng, and Qihuang Gong

Phys. Rev. Lett. **111**, 023006 — Published 9 July 2013

DOI: 10.1103/PhysRevLett.111.023006

Subcycle dynamics of Coulomb asymmetry in strong elliptical laser fields

Min Li,[1] Yunquan Liu,[1,*] Hong Liu,[1] Qicheng Ning,[1] Libin Fu,[2,3] Jie Liu,[2,3] Yongkai Deng,[1] Chengyin Wu,[1] Liangyou Peng,[1] Qihuang Gong[1,†]

[1]*Department of Physics and State Key Laboratory for Mesoscopic Physics, Peking University, Beijing 100871, People's Republic of China*

[2]*National Key Laboratory of Science and Technology on Computation Physics, Institute of Applied Physics and Computational Mathematics, 100088 Beijing, People's Republic of China*

[3]*Center for Applied Physics and Technology, Peking University, 100084 Beijing, People's Republic of China*

We measure photoelectron angular distributions of noble gases in intense elliptically polarized laser fields, which indicate strong structure-dependent Coulomb asymmetry. Using a dedicated semiclassical model, we have disentangled the contribution of direct ionization and multiple forward scattering on Coulomb asymmetry in elliptical laser fields. Our theory quantifies the roles of the ionic potential and initial transverse momentum on Coulomb asymmetry, proving that the small lobes of asymmetry are induced by direct ionization and the strong asymmetry is induced by multiple forward scattering in the ionic potential. Both processes are distorted by the Coulomb force acting on the electrons after tunneling. Lowering the ionization potential, the relative contribution of direct ionization on Coulomb asymmetry substantially decreases and Coulomb focusing on multiple rescattering is more important. We do not observe evident initial longitudinal momentum spread at the tunnel exit according to our simulation.

PACS numbers: 32.80.Rm, 31.90.+s, 32.80.Fb, 32.80.Wr

Strong laser field ionization now provides a sophisticated method to image and probe the atomic and molecular quantum processes. As the basic processes, electron direct tunneling and rescattering lie in the very heart of attosecond physics [1]. Both direct tunneling and rescattering effects have been successfully used to resolve molecular orbitals [2, 3]. The advances in strong field physics have opened a window to precisely measure the delay time and initial coordinates of quantum tunneling [4, 5]. Recently, the use of elliptically polarized laser light fields has added more dimensions to study strong laser field ionization and has attracted particular attention [6-13], which gives rise to more features and properties that are not accessible with a linearly polarized laser field.

The Coulomb focusing effect is crucial for strong field single [14, 15] and double [16] ionization of atoms because of electron rescattering in linearly polarized laser fields [17, 18]. The typical signature of Coulomb field on above-threshold ionization in an elliptically polarized field has been shown experimentally [6, 8], manifested in the lack of the fourfold symmetry of photoelectron angular distributions with respect to the both main axes of polarization ellipse that is predicted by the PPT theory (Perelomov, Popov and Terent'ev) [19] and Strong-Field-Approximation [20]. Indeed, in the formation of Coulomb asymmetry by both direct ionization and rescattering processes, the role of ionic potential should not be ignored. Disentangling this effect from Coulomb asymmetry remains a key issue for us to understand the physics of strong field ionization.

In this Letter, we focus on photoelectron angular distributions of noble gases in intense elliptically polarized laser fields with a small ellipticity. With a semiclassical model, we study subcycle dynamics of Coulomb asymmetry on photoelectron angular distributions. We have decoupled the contributions of direct ionization and multiple forward scattering on Coulomb asymmetry in elliptical laser fields. We show that the tunneling time and initial transverse momentum have dominant roles on Coulomb asymmetry. By measuring photoelectron angular distributions for several noble gases at the same laser intensity, we show that, decreasing the ionization potential, the relative contribution of direct ionization will substantially decrease and Coulomb asymmetry will be dominated by multiple forward scattering. Interestingly and importantly, without considering the initial longitudinal momentum spread at the tunneling exit, we achieve a good agreement between the semiclassical simulations and experimental results.

We performed the experiments using 25fs, 795nm pulses from a Ti:Sa laser system with 3 kHz repetition rate, amplified pulse energy up to 0.8mJ. We measured photoelectron angular distributions with a reaction microscope (REMI) [21, 22] (for the principle see [23]) with photoelectron momentum resolution ~0.05 a.u. (atomic units) along the time-of-flight direction and ~0.08 a.u. along the transverse direction. The electric (~10 V/cm) and magnetic (~10 G) fields were applied along the time-of-flight axis. Ions and electrons were measured with two position-sensitive microchannel plate (MCP) detectors respectively. From the time-of-flight and position on the detectors, the full momentum vectors of particles were calculated. In the off-line analysis, the photoelectrons were selected in coincidence with their singly charged parent atomic ions. Since the spectrometer of REMI loses momentum resolution of ions that is perpendicular to the time-of-flight direction while increasing the atomic mass, instead of measuring the ion momentum distribution, we measured the photoelectron angular distributions of noble gases in strong elliptically polarized laser fields. The laser ellipticity was monitored by a broad-band quarter-wave plate.

The measured two-dimensional photoelectron momentum distribution in the polarization plane for Ne at intensity of 3×10^{14}W/cm^2 with a small ellipticity ~0.25 is shown in Fig. 1a. For ellipticity < 0.3, the formation of the asymmetric four peaks is a prominent feature in the momentum distribution for Coulomb asymmetry [13]. The major axis is along *z* direction, the minor axis is along *x* direction, and *y* is the laser propagation direction. At such a laser intensity, the Keldysh parameter γ ($\gamma=\sqrt{2I_p/U_p}$, I_p: the ionization potential, U_p: the ponderomotive potential, $U_p=E_0^2/4\omega^2$, E_0: field amplitude; ω: field frequency, atomic units are used throughout otherwise specified) increases from ~0.8 to about ~3.2, when the instantaneous field rotates from the major axis to the minor axis for Ne.

In order to achieve deep insight into Coulomb asymmetry, we perform three dimensional semiclassical electron ensemble simulations. Briefly, in the model the electron initial position along the laser polarization direction is derived from the Landau's effective potential theory [24]. The tunneled electrons have a Gaussian-like distribution on the transverse momentum perpendicular to the instantaneous laser field and *zero* longitudinal momentum along the instantaneous laser field. Each electron trajectory is weighted by the ADK ionization rate $W(t_0,v_\perp^i)=W_0(t_0)W_1(v_\perp^i)$[25], in which

$W_1(v_\perp^i) \propto v_\perp^i[\sqrt{2I_p}/|\mathbf{E}(t_0)|]\exp\left[\sqrt{2I_p}(v_\perp^i)^2/|\mathbf{E}(t_0)|\right]$ depends on the distribution of initial transverse velocity $v_\perp^i$ and $W_0(t_0) = |\left(2I_p\right)^2/|\mathbf{E}(t_0)||^{2/\sqrt{2I_p}-1}\exp\left[-2\left(2I_p\right)^{3/2}/|3\mathbf{E}(t_0)|\right]$ depends on the instantaneous laser field $\mathbf{E}(t_0)$ at the instant that the electrons release and I_p (the ionization potential). The elliptically polarized laser field is given by $\mathbf{E}(t) = E_0 f(t)[\cos(\omega t+\phi)\mathbf{z} + \varepsilon\sin(\omega t+\phi)\mathbf{x}]$, where *f*(t) is the pulse envelop, E_0 and ω are the amplitude and frequency of laser field respectively, and ε is the ellipticity. After tunneling the electron evolution in the combined oscillating laser field and Coulomb field is solved via the Newtonian equation, $\ddot{\mathbf{r}} = -\mathbf{r}/r^3 - \mathbf{E}(t)$, *r* is the distance between electron and nucleus. To solve the Newtonian equations more precisely close to nucleus, we use the explicit method that can automatically select the solution algorithm when solving ordinary differential equations [26]. The simulated photoelectron momentum distribution for Ne at an intensity of 3×10^{14} W/cm^2 is illustrated in Fig. 1b, in which we use a Gaussian envelope *f*(t) with a FWHM width of 25 fs. The asymmetric distribution of photoelectrons with four lobes can be clearly observed in two-dimensional photoelectron momentum distributions in Fig. 1. The experimental (dotted line) and simulated (solid line) momentum-integrated angular distributions of Ne are also shown in Fig. 2a. The simulated photoelectron momentum distribution agrees with the experiment quantitatively.

Now we pay our attention on subcycle dynamics of Coulomb asymmetry by disassembling two-dimensional momentum distribution. To do that, we then use a half-trapezoidal pulse with constant amplitude seven cycles ramping off within three cycles, in which all of electrons tunnel in the first laser cycle. The electron momentum-integrated angular distribution with respect to the ionization time window of (0.25*T*, 0. 75*T*) (the instantaneous field rotates from the minor axis for a half laser cycle, here *T* is the laser cycle) is shown in Fig. 2b. One can observe two groups of electrons marked with A and B respectively. The area A corresponds to the events with emission angle ~30^o in the tunneling time of (0.25*T*, 0.48*T*) and the area B corresponds to the events with emission angle ~150^o in the tunneling time of (0.48*T*, 0.75*T*) respectively. The separation of tunneling time is based on careful analysis on electron trajectories (details are described in [27]). We can clearly identify that the

electrons of area A are mainly from direct ionization. Those electrons are ionized when the instantaneous field rotates before the major axis within a quarter of laser cycle and will be pulled away directly by the laser field. However, those electrons are ionized after $0.48T$ can be driven back towards the parent ion. The time shift from $0.5T$ (the field maximum) is due to Coulomb potential. Depending on initial tunneling coordinates, those electrons will be scattered forward or backward by the ionic potential in the oscillating field. In an elliptically polarized field, because of the field component along the minor axis, the ionized electron will acquire a lateral drift motion with respect to the major polarization axis, and will substantially suppress the backward scattering for those rescattered electrons with small impact parameter. Accordingly, most of electrons of area B will miss the direct impaction on nucleus and will be scattered forward with a small scattering angle. Those electrons may experience forward scattering many times at their subsequent multiple returns in a long pulse. We can separate this process and direct ionization by dissecting the two-dimensional momentum distributions. The two-dimensional photoelectron momentum distributions of group A and group B producing in the first half cycle are shown in Fig 2c and 2d respectively. By analyzing subcycle ionization dynamics, we have decoupled the contribution of direct ionization and multiple forward scattering on Coulomb asymmetry. Obviously, the directly ionized electrons contribute to the small lobes and those multiple forward scattering electrons contribute to the main lobes of Coulomb asymmetry.

Different with linearly polarized field, the initial transverse momentum along the minor and major polarization axis is not symmetrical for an elliptically polarized field. Thus, it is very necessary to consider the role of the initial transverse velocity $\mathbf{v}_\perp$ of the tunneled electrons on Coulomb asymmetry. In Figs. 3a, and 3b, we show the momentum-integrated angular distribution with respect to the initial transverse momentum along the minor axis $\boldsymbol{x}$ and laser propagation direction $\boldsymbol{y}$, respectively. Because there is non-zero field component along the minor axis, depending on the instantaneous field direction, the tunneled electrons with positive and negative initial transverse momentum v_x have different contributions to photoelectron angular distribution. On the other hand, since there is no laser field force along the laser propagation direction, the contribution of the transverse momentum along this direction on Coulomb asymmetry is symmetric.

In order to see details of the ionic potential effect on the electrons of direct ionization and multiple forward scattering, we further show the final transverse momentum distribution along the laser propagation direction with respect to the tunneling time in Fig. 3c. Both the final electron transverse momentum distributions along the laser propagation direction of direct ionization and multiple forward scattering are smaller than the initial transverse momentum at the tunnel exit. Clearly, depending on the tunneling time, the electrons experience different strength of Coulomb focusing. Since the rescattering part will experience stronger Coulomb focusing effect, the width of final transverse momentum of the rescattering part is much narrower than that of directly ionized electrons.

We have further measured the photoelectron angular distributions for Ar, Kr and Xe targets at the ellipticity ~0.25 at the same intensity of 1.5×10^{14}W/cm^2, as shown in Fig. 4a. From the experimental results, we can find the four-lobe structure in the angular distribution becomes less evident when the ionic potential is lower, e.g., the small lobes corresponding to direct ionization can hardly be seen for Xe atoms. Decreasing the ionization potential, the contribution of direct ionization on Coulomb asymmetry is substantially reduced. Simultaneously, the main emission angle is shifted to the major axis when decreasing the ionization potential. The simulated momentum-integrated angular distributions for Ar, Kr and Xe targets are shown in Fig. 4b using a Gaussian envelope f(t) with a FWHM width of 25 fs.

One can find that Coulomb asymmetry is dominated by multiple forward scattering for the targets with lower ionization potential. Since the tunnel exit can be approximately given by I_p / E_0 for the short-range potential [8], the electron is released at a shorter distance from the ion to the tunnel exit point for a smaller ionization potential at the same field strength, and thus the Coulomb potential has a more active attraction on electrons for the targets with lower ionization potential. As a result, an atom with lower ionization potential has a narrower tunneling-time window for direct ionization and rescattering occurs earlier (indicated with white dashed lines in Fig. 3c for Ne and 3d for Xe). This leads to the suppression of the small lobes in the angular distribution for the atoms with lower ionization potential, which is consistent with the experimental results. On other hand, Coulomb focusing effect becomes more important on electrons multiple forward scattering for atoms with lower ionization potential because the tunneled electrons can reach more close to

nucleus in multiple forward scattering. As seen in Fig. 3d, the final transverse momentum along laser propagation direction of electrons with multiple forward scattering is much narrower for Xe at an intensity of 1.5×10^{14}W/cm^2 with the ellipticity ~0.25, revealing strong Coulomb focusing effect.

Including the Coulomb force at the tunnel exit, the momentum components along the major and minor axis for the dominant emission angle are approximately given by $p_z = -\pi\sqrt{2z_e / E_0}\big/(4z_e^2)$ [8], $p_x = \varepsilon E_0 / \omega$ if ignoring the initial momentum. Taking the tunnel exit point with a form of $z_e = (I_p + \sqrt{I_p^2 - 4(1-\sqrt{2I_p}/2)E_0})/(2E_0)$ that is developed in parabolic coordinates [5], the calculated emission angle $\theta = \cos^{-1}(p_z / \sqrt{p_x^2 + p_z^2})$ is much smaller than the measurement, e.g., for Xe, the estimated angle is about ~140^o, while the simulation and experiment are near 170^o. Indeed, the emission angle depends on both the ionization potential and initial transverse momentum in the polarization plane. As seen in Fig. 3a, non-zero initial transverse momentum along the minor axis will strongly modify the photoelectron angular distribution. The effective final momentum along this direction should be $p_x = \varepsilon E_0 / \omega \pm v_{x0}$ (“$\pm$” for positive and negative initial transverse momentum respectively). For the main lobe of photoelectron angular distribution, the effective initial transverse momentum along the minor axis v_{x0} is opposite with the field momentum $\varepsilon E_0 / \omega$ and is comparable with the field momentum. The final momentum along the minor axis p_x becomes much small, and thus the emission angle will be much larger than above estimation. On the other hand, the momentum along the major axis p_z increases slightly when decreasing the ionic potential at the same laser intensity. The Coulomb focusing effect becomes stronger for atoms with lower ionization potential, and thus the emission angle will shift further to the major axis.

We should note that, without taking into account of the initial longitudinal momentum spread at the tunnel exit, our semiclassical simulation can reproduce the experimental results. To verify that, we further simulate the recent experimental results on the ellipticity-dependence angular distribution for He in [13]. Without including the initial longitudinal momentum, the calculated ellipticity-dependence angular distribution agrees with the experiment for He very well, as seen in Fig. 5a. In

Fig. 5b, for a small ellipticity $\varepsilon = 0.3$, the angular distribution reveals four lobes and for $\varepsilon = 0.8$, the angular distribution shows double lobes. This is in contrast with the calculation in [13], where it includes the initial longitudinal momentum spread as large as ~ 1 a.u..

In conclusion, we have presented the combined experimental and theoretical study on photoelectron angular distributions of noble gases in strong elliptical laser fields. With the semiclassical simulation, we have analyzed subcycle dynamics on Coulomb asymmetry. Our study shows that it is possible to decouple the basic steps of direct ionization and multiple forward scattering and to resolve the role of the ionic potential using an elliptical laser field, which are vey important in a broad range of strong field phenomena. Our data quantify one aspect of how ionic potential will become more important for atoms and molecules with lower ionization potential. The direct ionization is much suppressed and electron multiple forward scattering dominates Coulomb asymmetry for atoms with lower ionization potential. Our semiclassical simulation indicates that the initial longitudinal momentum spread at the tunnel exit is less evident.

This work is supported by the 973 program (No. 2013CB922403), the NSFC (Nos. 61078025, 11121091, and 11134001), the NCET and SRF for ROCS in University from Ministry of Education. Y. L. acknowledges the support by the National Science Fund for Distinguished Young Scholars in China (No. 11125416).

*Yunquan.liu@pku.edu.cn

†qhgong@pku.edu.cn

References

[1] P. B. Corkum and F. Krausz, Nature Phys. **3**, 381(2007).

[2] M. Meckel, D. Comtois, D. Zeidler, A. Staudte, D. Pavičić, H. C. Bandulet, H. Pépin, J.C. Kieffer, R. Dörner, D.M. Villeneuve, and P.B. Corkum, Science **320**, 1478(2008).

[3] H. Akagi. T. Otobe, A. Staudte, A. Shiner, F. Turner , R. Dörner, D. M. Villeneuve, P. B. Corkum, Science **325**, 1364(2009)

[4] P. Eckle, A. N. Pfeiffer, C. Cirelli, A. Staudte, R. Dörner, H. G. Muller, M. Büttiker, and U. Keller, Science **322**, 1525(2008).

[5] A. N. Pfeiffer, C. Cirelli, M. Smolarski, D. Dimitrovski, M. Abu-samha, L. B. Madsen, and U. Keller, Nature Phys. **8**, 76(2012).

[6] M. Bashkansky, P.H. Bucksbaum, and D.W. Schumacher, Phys. Rev. Lett. **60**, 2458(1988).

[7] G. G. Paulus, F. Zacher, and H. Walther, A. Lohr, W. Becker, and M. Kleber, Phys. Rev. Lett. **80**, 484(1998).

[8] S.P. Goreslavski, G.G. Paulus, S.V. Popruzhenko, and N.I. Shvetsov-Shilovski, Phys. Rev. Lett. **93**, 233002(2004).

[9] C. Liu and K.Z. Hatsagortsyan, Phys. Rev. A **85**, 023413(2012).

[10] N. I. Shvetsov-Shilovski, D. Dimitrovski, and L. B. Madsen, Phys. Rev. A **85**, 023428(2012)

[11] D. Shafir, B. Fabre, J. Higuet, H. Soifer, M. Dagan,D. Descamps, E. Mevel, S. Petit, H. J. Worner, B. Pons, N. Dudovich, and Y. Mairesse, Phys. Rev. Lett. **108,** 203001(2012).

[12] X. Wang and J. H. Eberly, Phys. Rev. Lett. **103**, 103007 (2009).

[13] A.N. Pfeiffer, C. Cirelli, A.S. Landsman, M. Smolarski, D. Dimitrovski, L.B. Madsen, and U. Keller, Phys. Rev. Lett. **109**, 083002 (2012).

[14] D. Comtois, D. Zeidler, H. Pépin, J.C. Kiefer, D. M. Villeneuve, and P.B. Corkum, J. Phys. B **38**,1923(2005).

[15]A. Rudenko, K. Zrost, T. Ergler, A. B. Voitkiv, B. Najjari, V. L. B. de Jesus, B. Feuerstein, C. D. Schröter, R. Moshammer, and J. Ullrich, J. Phys. B **38**, L191 (2005).

[16] Y. Liu, D. Ye, J. Liu, A. Rudenko, S. Tschuch, M. Dürr, M. Siegel, U. Morgner, Q. Gong, R. Moshammer, and J. Ullrich, Phys. Rev. Lett. **104**, 173002(2010).

[17] K. J. Schafer, B. Yang, L. F. DiMauro, and K. C. Kulander, Phys. Rev. Lett. **70**, 1599 (1993).

[18] P. Corkum, Phys. Rev. Lett. **71**, 1994 (1993).

[19] A.M. Perelomov, V. S. Popov, and M.V. Terent'ev, Zh.Eksp. Teor. Fiz. **51**, 309 (1966) [Sov. Phys. JETP **24**, 207 (1966)].

[20] S. Basile, F. Trombetta, and G. Ferrante, Phys. Rev. Lett. **61**, 2435 (1988); P. Krstic and M. H. Mittleman, Phys. Rev. A **44**, 5938 (1991).

[21] H. Liu, Y. Liu, L. Fu, G. Xin, D. Ye, J. Liu, X.T. He, Y. Yang, Y. Deng, C. Wu, Q. Gong, Phys. Rev. Lett. **109**, 093001(2012)

[22] M. Li, Y. Liu, H. Liu, Y. Yang, J. Yuan, X. Liu, Y. Deng, C. Wu, and Q. Gong, Phys. Rev. A **85**, 013414 (2012).

[23] J. Ullrich, R. Moshammer, A. Dorn, R. Dörner, L.Ph.H. Schmidt, and H.

Schmidt-Böcking, Rep. Prog. Phys. **66**, 1463(2003).

[24] L.D. Landau, and E. M. Lifshitz, *Quantum Mechanics* (Pergamon, Oxford,1977).

[25] A. M. Perelomov, V. S. Popov and V. M. Teren'ev, Zh. Eksp. Teor. Fiz. **52**,514 (1967) [Sov. Phys. JETP **25**, 336(1967)]; M. V. Ammosov, N. B. Delone and V. P. Krainov, Zh. Eksp. Teor. Fiz. **91**, 2008(1986) [Sov. Phys. JETP **64**, 1191(1986)]; N. B. Delone and V. P. Krainov, J. Opt. Soc. Am. B **8**, 1207(1991).

[26] Linda Petzold, Siam J. Sci. Stat. Compt. **4**, 136(1983).

[27] Supplementary material.

Figure captions:

Figure 1. The two-dimensional experimental (a) and simulated (b) photoelectron momentum distributions of Ne in an elliptically polarized laser field at an intensity of 3×10^{14}W/cm^2.

Figure 2. (a) The momentum-integrated angular distribution of Ne in an elliptical laser field (the ellipticity ~ 0.25) at an intensity of 3×10^{14}W/cm^2 of experiment (dotted) and simulation (solid). (b) The momentum-integrated angular distribution with respect to the tunneling time. The red solid line shows the field component along the major axis. Two groups of electrons marked A and B are mainly induced by direct ionization and multiple forward scattering, which are separated by the white dashed line. (c) and (d) show two-dimensional photoelectron momentum distributions of direct ionization and multiple forward scattering, respectively.

Figure 3. (a) and (b) show the momentum-integrated angular distributions with respect to the initial transverse velocities of along the minor axis and the laser propagation direction. (c) and (d) show the electron tunneling time with respect to the final transverse momentum along the laser propagation direction for Ne 3×10^{14}W/cm^2 and (d) for Xe 1.5×10^{14}W/cm^2 (the ellipticity ~0.25). The solid lines and dashed lines in (c) and (d) show the position of half maximum of p_y^{final} and the tunneling time when rescattering begins to occur, respectively, and the color scale is normalized to the maximum rate for each tunneling time.

Figure 4. The experimental (a) and simulated (b) momentum-integrated angular distributions of Ar, Kr and Xe (ellipticity ~0.25) at an intensity of 1.5×10^{14}W/cm^2.

Figure 5. (a) The simulated ellipticity-dependent momentum-integrated angular distribution for He. (b) The simulated angular distributions for two elliptical values. In the simulation, there is no initial longitudinal momentum included.

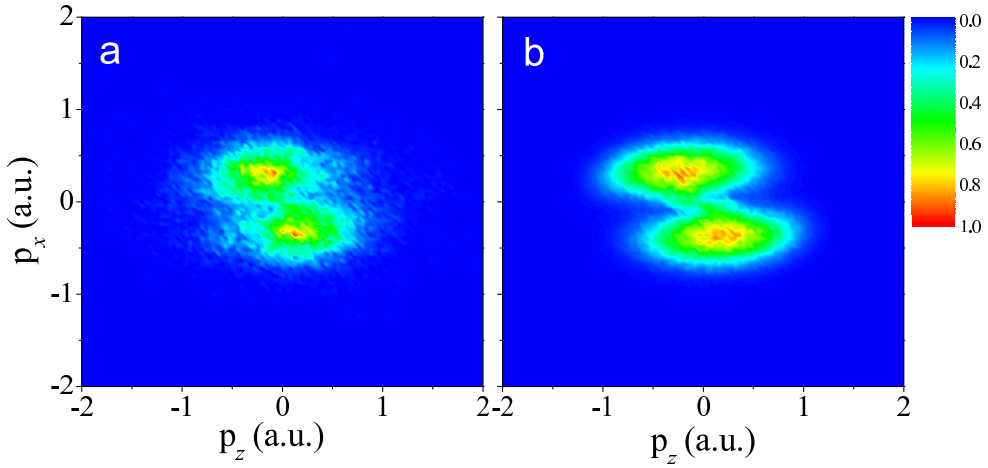

Figure 1 LZ13200 14MAY2013

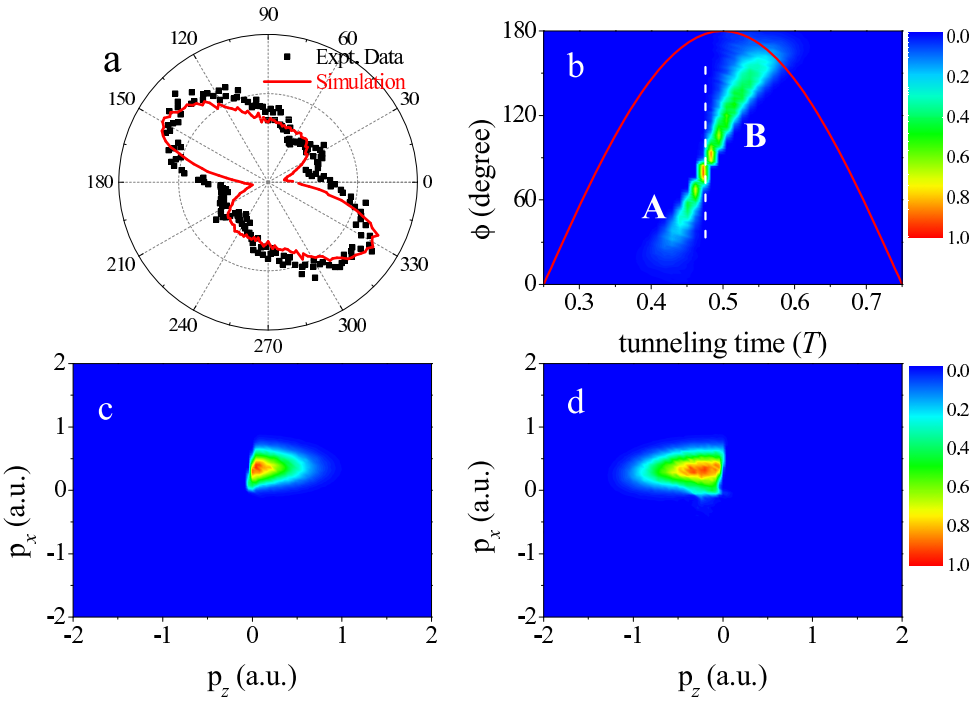

Figure 2 LZ13200 14MAY2013

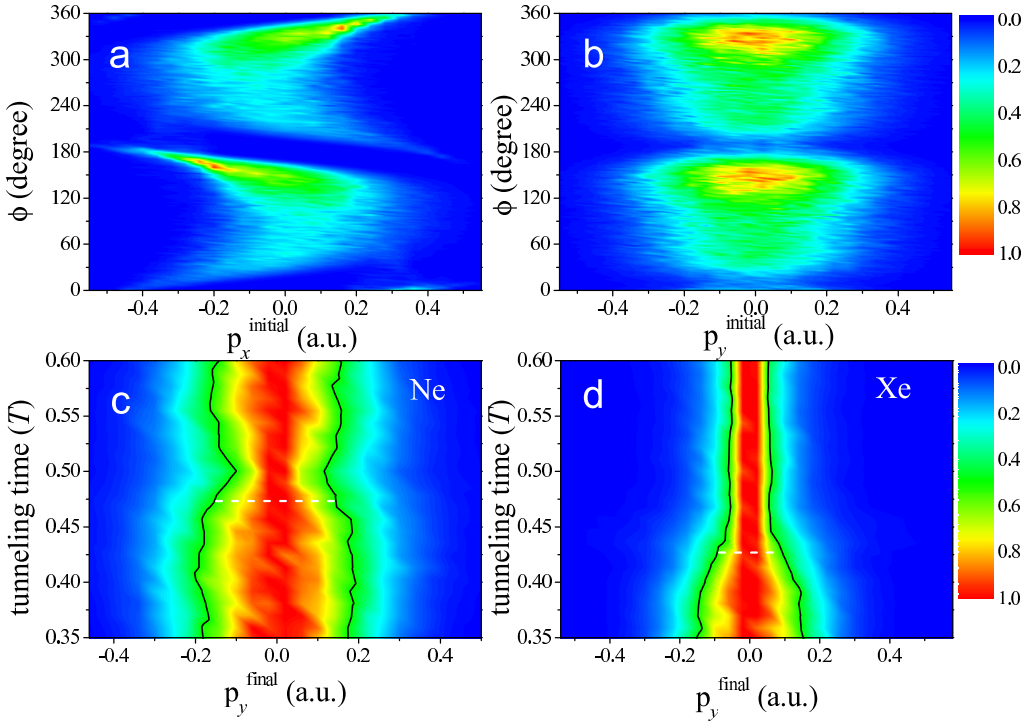

Figure 3 LZ13200 14MAY2013

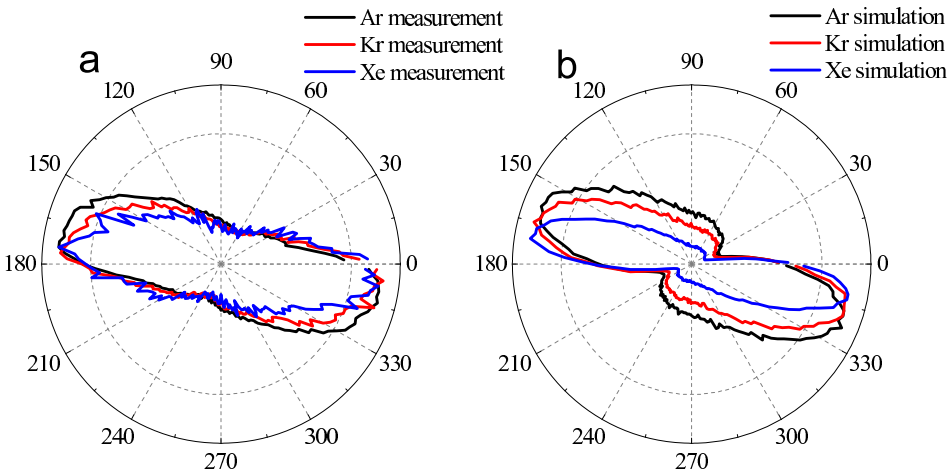

Figure 4 LZ13200 14MAY2013

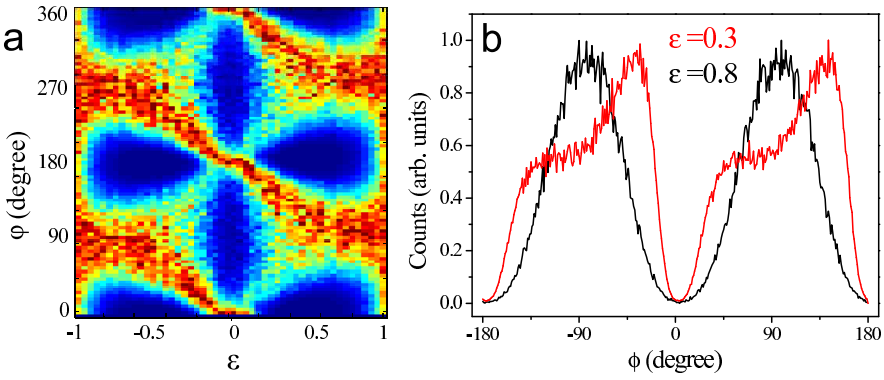

Figure 5 LZ13200 14MAY2013